Tellus (1985), *37A*, 56–76

Thermally-forced mean mass circulations in the Southern Hemisphere

By JOHN W. ZILLMAN, *Bureau of Meteorology, Melbourne, Victoria 3001, Australia,* and DONALD R. JOHNSON, *Department of Meteorology, Space Science and Engineering Center, University of Wisconsin, 1225 West Dayton Street, Madison, Wisconsin 53706, USA*

(Manuscript received June 6, 1983; in final form July 3, 1984)

ABSTRACT

The three-dimensional distribution of the thermally-forced time-averaged horizontal mass transport in isentropic coordinates is determined for the Southern Hemisphere from modeled diabatic heating fields. The model, based on the time-averaged isentropic continuity equation, specifies the horizontal mass transport in terms of the gradient of a mass transport potential on a vertical array of isentropic surfaces. The mass transport potential is derived by numerical solution of a two-dimensional Poisson equation on a hemispheric grid. The Southern Hemisphere heating fields are based on estimates of the normal summer and winter columnar radiative, latent and sensible heating and simplified models of their vertical apportionment.

The results highlight the role of radiative cooling over the cold elevated Antarctic ice cap, sensible heat flux from the warm circumpolar ocean and, in particular, the zonal and meridional contrasts of latent heat release in forcing large-scale mean mass circulations in the Southern Hemisphere. The inferred mass circulations include strong meridional (Hadley) and zonal (Walker) components in the tropical belt extending into the middle and high latitudes of the Southern Hemisphere. Of particular interest is a large toroidal mass circulation cell transporting heat away from the heavy rainfall belt lying southeast from Papua-New Guinea to regions of net radiative cooling to the east, west, north and south.

1. Introduction

The atmospheric general circulation has been studied from many viewpoints. The concept of direct solenoidally driven circulations in vertical planes based on the classical theorems of Bjerknes and Sandstrom (Bjerknes et al., 1933) has proven of considerable value in elucidating the basic thermodynamic nature of the atmospheric response to differential heating. Eckart (1960) and Riehl (1969) in particular exploit the pedagogical value of this elegant heat engine analogy to the general circulation. However, the complexities of the earth's rotation and the excitation of geostrophy so distort the simple thermally induced motions that observed mean circulation patterns associated with heat sources and sinks of planetary and continental dimensions have been found to be not readily explained by this model (Smagorinsky, 1953).

Following the recognition by Jeffreys (1933) that the poleward flux of absolute angular momentum needed to maintain the westerlies of middle latitudes could be accomplished by extratropical cyclones and waves, Priestley (1949), Starr (1951), and others demonstrated that the large-scale horizontal fluxes of momentum and energy could be satisfactorily derived from available upper air data. Thus began two decades of intensive study of the transfer of mass, momentum and energy by mean meridional circulations and transient and standing eddies. After some initial controversy (Rossby and Starr, 1949; Palmén, 1949; Riehl and Yeh, 1950), the eddies have assumed a fundamental role in our understanding of the maintenance of the atmospheric general circulation (e.g., Lorenz, 1967).

Implicit in all of this work is the knowledge that the atmosphere's motion is in response to large-scale differential heating. However, in latitudes where the earth's rotation is important, the scale of response corresponds to the scale of the quasi-horizontal waves. No large-scale response in extra-tropical latitudes corresponding to the scale of thermal forcing is isolated.

The broad purpose of this study is to identify the role of three-dimensional heat sources and sinks in forcing a time-averaged planetary-scale mass circulation in the Southern Hemisphere. The condition that such planetary-scale mass circulations must exist is inferred from the isentropic equation of continuity. Horizontal mass transport from a heat source to a heat sink must occur in upper isentropic layers while the mass transport must be from heat sink to heat source in lower isentropic layers in order to satisfy the continuity requirement that mass transport be upward through isentropic surfaces in the heat source region and downward in the heat sink region. An important additional constraint is that the isentropic mass circulation determines the sense and scale of the energy transport (Johnson and Townsend, 1981). Viewed in this context, one concludes that the mass and energy transports by the large-scale isentropic circulation are fundamentally important in the development of a basic theory for climate.

Our immediate purpose is to model the thermodynamic forcing of the planetary circulation in the Southern Hemisphere from climatic information and isolate the circulations that couple the major regions of diabatic heating and cooling. Specifically, the mass transport that couples the radiative cooling over the Antarctic ice cap, the heat flux from the warm circumpolar ocean and the meridional and zonal contrasts in latent heating associated with major deserts and rain belts is determined. This study compliments a similar study for the Northern Hemisphere by Otto-Bliesner and Johnson (1982).

Section 2 presents the framework for a diagnostic evaluation of the thermally-forced mass circulation. Section 3 assembles estimates of the isentropic mass distribution, radiation, precipitation, and boundary layer heating for the Southern Hemisphere and combines these quantities to produce maps of a forcing function for the horizontal mass transport.

The main results of the study are presented in Sections 4–6. The derived three-dimensional distributions of horizontal mass transport in January (summer) and July (winter) are presented in Section 4. Section 5 discusses the east-west component of the thermally forced mass circulations and their relation to the tropical Walker circulation. Section 6 analyzes the implied mean meridional circulation and its variation with longitude.

Finally, in Section 7 the energy transport by quasi-steady thermally-forced mass circulations and the energy balance of the Southern Hemisphere are briefly examined.

2. Formulation

The equation of continuity in isentropic coordinates is

$$\frac{\partial}{\partial t_\theta}(\rho J_\theta) + \nabla_\theta \cdot (\rho J_\theta \mathbf{U}) + \frac{\partial}{\partial \theta}(\rho J_\theta \dot{\theta}) = 0, \tag{1}$$

where J_θ is the Jacobian of transformation from height to potential temperature. If the continuity equation is averaged over an appropriate period of time such that the mass distribution $(\overline{\rho J_\theta})$ may be regarded as steady, (1) reduces to

$$\nabla_\theta \cdot (\overline{\rho J_\theta \mathbf{U}}) = -\frac{\partial}{\partial \theta}(\overline{\rho J_\theta \dot{\theta}}), \tag{2}$$

where the overbar denotes temporal averaging. Physically (2) states that, the divergence of the time averaged horizontal mass transport on an isentropic surface is directly coupled to the vertical divergence of the time-averaged vertical mass transport.

With the horizontal mass transport expressed as the sum of irrotational (χ) and rotational (ψ) components according to Helmholtz's theorem

$$\rho J_\theta \mathbf{U} = \nabla_\theta \chi + \mathbf{k} \times \nabla_\theta \psi, \tag{3}$$

the continuity equation (2) takes the form

$$\nabla_\theta^2 \bar{\chi} = -\frac{\partial}{\partial \theta}(\overline{\rho J_\theta \dot{\theta}}) = F(\lambda, \phi, \theta), \tag{4}$$

where $F(\lambda, \phi, \theta)$ is a forcing function determined by the three-dimensional distribution of heating. The Poisson equation (4) may be solved for the distribution of the potential $\bar{\chi}$ given the distribution of the forcing function on the right hand side, along with appropriate boundary conditions. The forcing function in (4) is directly related to the diabatic heating distribution. Its importance stems from the constraint that for the time-averaged state the time-averaged irrotational component of the horizontal mass transport is directly and uniquely coupled to the diabatic heating. The time-averaged mass stream function that determines the rotational component of the horizontal mass transport remains independent of thermodynamically forced component of the transport. The Poisson equation for $\bar{\chi}$ was solved numerically by a finite difference analogue over a regular latitude–longitude grid by the method of successive over-relaxation. For the Southern Hemisphere study, a regular five-degree latitude–longitude grid extending from the South Pole to 25° N was employed. Vertical derivatives are computed over 10 K layers so that the distribution of $\bar{\chi}$ represents a layer averaged transport centered on the intermediate isentropic surface.

Several types of boundary conditions occur. For isentropic surfaces which are above ground everywhere between the South Pole and 25° N, $\bar{\chi}$ is set equal to zero at 25° N (Dirichlet boundary condition), a condition of zero zonal mass transport by the irrotational component along 25° N. Although this is unlikely to be a realistic approximation, the boundary of integration is well removed from the region of primary interest of this study and the transport patterns in the Southern Hemisphere should not be strongly affected. The second important type of boundary condition occurs with isentropes which, north of some latitude circle within the grid, never rise above the ground at any longitude. In this case both $\bar{\chi}$ and its normal derivative are set equal to zero on the boundary since there can be no mass transport out of the region on underground isentropes. This boundary condition is consistent with the convention that for a hydrostatic atmosphere the mass within "underground" isentropic layers is zero (Dutton and Johnson, 1967).

The finite difference and relaxation schemes were tested on a number of analytical and other fields with known solutions and were found to be entirely satisfactory. A convergence criterion of 0.2×10^6 kg K^{-1} s^{-1} was used. Additional details of the computational grid, finite difference equations relaxation scheme boundary conditions and tests of convergence are given in the original study by Zillman (1972a).

3. Modeled diabatic heating

In modeling the forcing function (4) the vertical mass transport is approximated through the thermodynamic equation

$$\dot{\theta} = \pi^{-1} Q \tag{5}$$

and the hydrostatic equation

$$\rho J_\theta = g^{-1}\, \partial p / \partial \theta \tag{6}$$

by

$$\overline{\rho J_\theta \dot{\theta}} = -\,(g\bar{\pi})^{-1} \frac{\partial \bar{p}}{\partial \theta}\, \bar{Q}. \tag{7}$$

π is the Exner function and Q is the specific rate of heat addition.

The error in approximating the diabatic mass flux in (7) from the neglect of covariance terms cannot be assessed from the data utilized in this study nor from current data, since no direct observations of heating are available. The validity of the results largely rests upon agreement with the results of Townsend (1980) and Johnson and Townsend (1981) who derived the distributions of heating from observations of mass transport using FGGE data. The large-scale patterns of heating and mass circulations in their study are similar to the results of this analysis. The assumptions used in this analysis, though, are not imposed in their study where $\rho J \dot{\theta}$ is estimated from the horizontal divergence of the observed isentropic mass transport. If violations of the assumptions used in this study seriously compromised the analysis to determine the isentropic mass circulation, the results would be dissimilar. In modeling of the thermodynamically forced mass circulations from climatic data for the Northern Hemisphere, Otto-Bliesner and Johnson (1982) used the same approximations without seemingly compromising their results.

The diabatic heating Q includes contributions from net radiative flux convergence Q_R, latent heat release by condensation Q_L and convergence of the small-scale vertical eddy flux of sensible heat Q_H such that

$$\bar{Q} = \bar{Q}_R + \bar{Q}_L + \bar{Q}_H. \tag{8}$$

Thus the forcing function F is divided into separate radiative, latent and sensible heating components according to

$$F = F_R + F_L + F_H. \tag{9}$$

Since the mean diabatic heating for the radiative, latent and sensible heating components cannot be determined directly from observations, estimates of the forcing function through the various approximations and models were assembled from climatological information. The main features of the approach are summarized as follows:

(i) The time averaged mass $\overline{\rho J_\theta}$ equal to $[-\partial(\bar{p}/g)/\partial\theta]$ is estimated from isobarically-averaged data as $[-g\,\partial[\bar{\theta}(p)]/\partial p]^{-1}$.
(ii) $(\overline{\theta/T})$ is estimated from isobarically-averaged data as $[1000/p(\bar{\theta}(p))]^{\kappa}$.
(iii) $\bar{Q}_R(\theta)$ and $Q_L(\theta)$ are interpolated from isobaric profiles of radiative and latent heating by assigning to each isentropic surface the mean heating rates at the pressure whose mean potential temperature is that of the selected isentrope i.e. $\bar{Q}(\theta) = \bar{Q}[\bar{\theta}(p)]$.
(iv) The sensible heating component for the boundary layer is estimated independently using a simple model for vertical apportionment of heating.
(v) The resulting estimates of mean diabatic heating in isentropic coordinates are adjusted for consistency with the assumption of steady mass distribution.

A detailed description of this climatological approach for estimation of the mass distribution, the radiative, latent and sensible heating contributions to the forcing function, the adjustment for steady state, and the spatial distribution of the forcing function on selected isentropic surfaces for the Southern Hemisphere is presented in Zillman (1972a). A similar approach was used by Otto-Bliesner and Johnson (1982) in their Northern Hemisphere study. In view of the details presented in these studies, only a brief description of the climatological approach is now presented. For specific details readers should refer to the references just noted.

3.1. *Mass distribution*

Estimates of $\bar{p}(\lambda,\phi,\theta)$ and $\overline{\rho J_\theta}(\lambda,\phi,\theta)$ for the Southern Hemisphere were based principally on the atlas tabulations of normal January and July temperatures at the 850, 700, 500, 300, 200 and 100 mb levels (Taljaard et al., 1969) and meridional cross sections at 30-degree intervals of longitude (Crutcher et al., 1971). Since radiosonde information is recorded at standard isobaric levels (850, 700, 500 mb, . . .), the time-average $\bar{\theta}(\lambda,\phi,p)$ was inverted to $p[\lambda,\phi,\bar{\theta}(p)]$ from which $\bar{p}(\lambda,\phi,\theta)$ was estimated by interpolation.

Fig. 1 summarizes the main features of the inferred isentropic mass distribution in the form of zonally-averaged meridional cross sections of $\overline{\rho J_\theta}$ for January and July. Note, however, that in contrast with the companion study for the Northern Hemisphere (Otto-Bliesner and Johnson, 1982), where $\overline{\rho J_\theta}$ and other quantities are presented on a latitude–potential temperature grid, the corresponding quantities defined in the isentropic coordinate system are, in this study, mapped back into an isobaric coordinate representation of the zonally-averaged structure, $(\phi, \bar{p}[\bar{\theta}(p)])$.

3.2. *Radiative heating*

While three-dimensional evaluations of net radiative heating have been made for the Northern

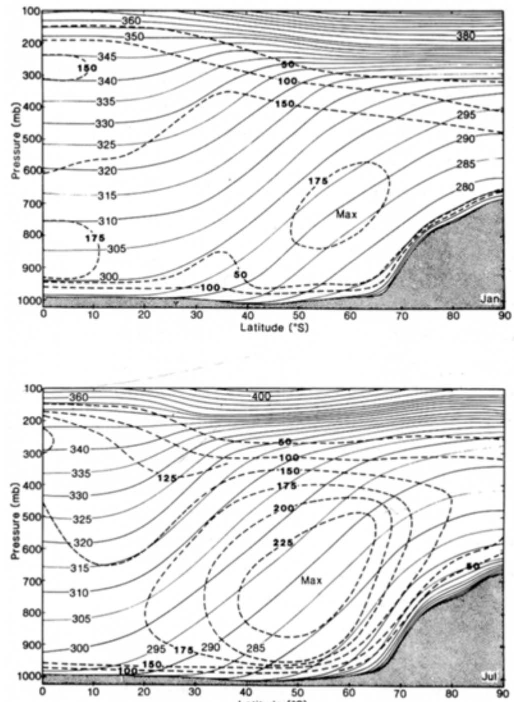

Fig. 1. Zonally-averaged mass-potential temperature distribution in January (top) and July (bottom) after being mapped into pressure coordinates. The heavy broken lines are isopleths of the zonally-averaged mass distribution, $[\rho J_\theta]$, in units of kg m^{-2} K^{-1}. The solid lines are isentropes (K).

Hemisphere (e.g., Katayama, 1967) much less detailed information is available for the Southern Hemisphere. The profiles of net radiative heating were assembled as follows. The zonally-averaged columnar shortwave heating estimates of Sasamori et al. (1971) were distributed with pressure according to the findings of Dopplick (1970) except over Antarctica in January where Dopplick's (1970) heating estimates as given were accepted. For the longwave radiative cooling, the zonally-averaged columnar estimates of Sasamori et al. (1971) were apportioned vertically according to Dopplick (1970) for the tropical and middle latitudes. Over Antarctica in July the adopted longwave cooling was based largely on radiometersonde data (White and Bryson, 1967; Kuhn et al., 1967; Schwerdtfeger, 1969). The results for the zonally-averaged net radiative heating prepared for each five degrees of latitude are presented in Fig. 2. In view of the lesser significance of zonal variations of radiative heating in comparison with latent heating, the meridional profile was assumed to be representative of the complete latitude circle.

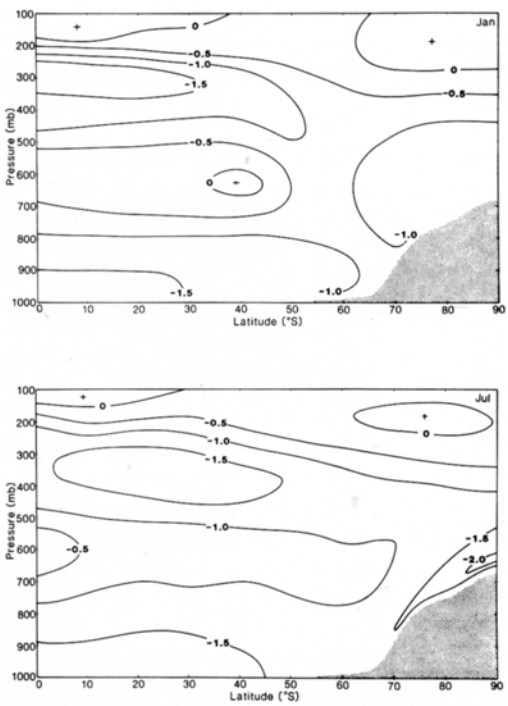

Fig. 2. Net radiative heating as a function of latitude and pressure for January (top) and July (bottom) in units of degrees per day.

3.3. *Latent heating*

In estimating the latent heating component $\overline{Q_L}(\lambda, \phi, \theta)$ the spatial distribution of the columnar (i.e., vertically integrated) latent heating is modeled first, after which the apportionment of the heating is distributed in the vertical. Let

$$\overline{Q_L} = c_p \eta L \bar{P}, \tag{10}$$

where $\bar{P}(\lambda, \phi)$ is the climatological mean precipitation, L is the latent heat of condensation and $\eta(p)$ is a weighting factor which describes the vertical apportionment of the columnar heating $L\bar{P}$. In order to ensure that the three-dimensional heating fields were consistent with estimates of the zonally-averaged heating, the various climatological maps were adjusted and revised in the light of the information available at the time when this study was conducted. Sellers' (1965) latitudinal distribution of mean annual precipitation was apportioned seasonally by adopting Möller's (1951) distributions over land and adjusting his oceanic values upward by a factor which varied with latitude between 1.1 and 1.4. This produced seasonal profiles essentially identical with Newton's (1972) latitudinal distributions but brought the spatial distribution into conflict with the records of several island stations where a negative "island effect" seemed unlikely. A process of successive adjustment in areas of lowest confidence, smoothing and computation of zonal averages was then performed using maps of mean January and July cloud cover from satellite data, monthly, seasonal and annual precipitation statistics, and graphs of the seasonal distribution of precipitation for key stations. Additional details and a complete list of references to the climatological sources of the information are given by Zillman (1972a). The columnar latent heat release (W m^{-2}) was computed from the resulting precipitation maps by multiplying the precipitation values (centimeters of water per day) by 289.3 equatorward and 328.0 poleward of the mean position of the freezing isotherm. The smoothed patterns for January and July are shown in Fig. 3. In view of the many sources of uncertainty in specifying the vertical distribution of the latent heat release, a simple scheme was adopted. The vertical apportionment was treated as a function of season and latitude only. Smooth profiles were prepared for each five degrees of latitude from the equator to 40° S based on the layer estimates of Vincent (1969). Poleward of

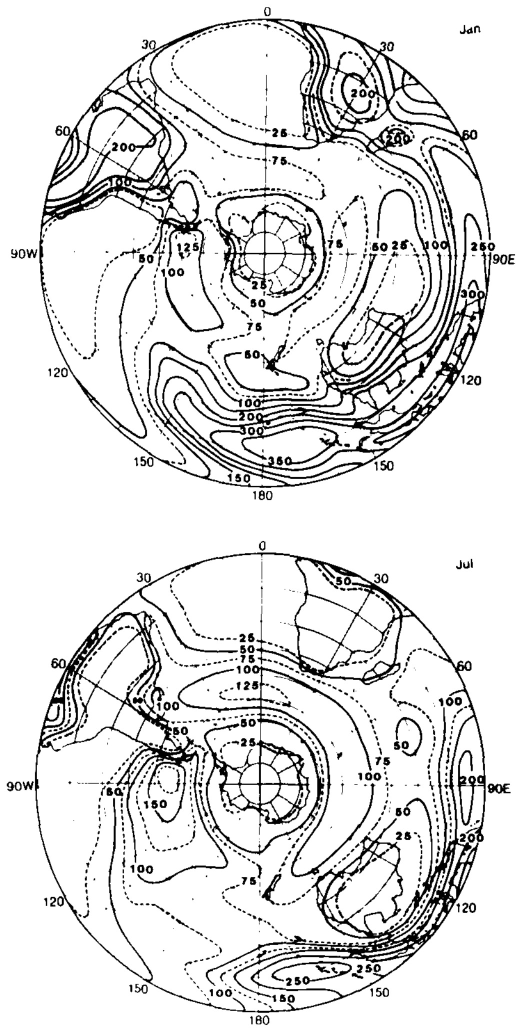

Fig. 3. The vertically integrated latent heat release for January (top) and July (bottom) in units of W m^{-2}.

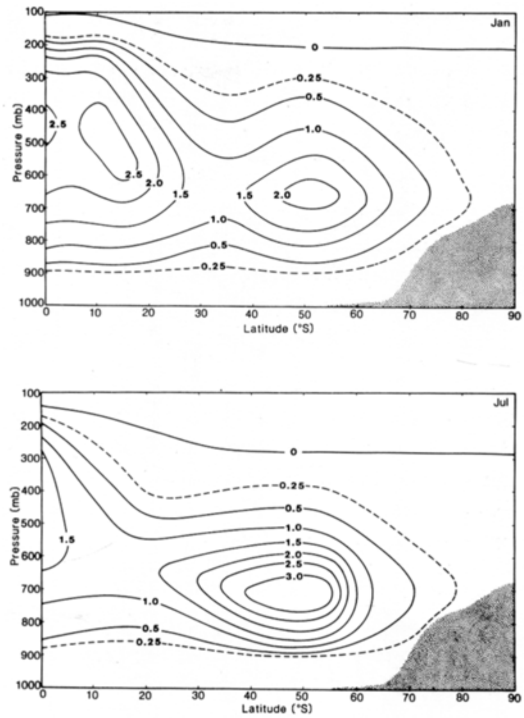

Fig. 4. Zonally-averaged latent heating as a function of latitude and pressure for January (top) and July (bottom) in units of degrees per day.

40° S the vertical apportionment was held constant. Values of η were thus derived for each isentropic surface at intervals of five degrees of latitude. The resulting zonally-averaged cross sections of latent heating are shown in Fig. 4.

3.4. *Sensible heating*

In this study the sensible heating to the planetary scale is assumed to be confined to the boundary layer and determined by the energy flux through the earth–atmosphere interface. The adopted distribution of the surface sensible heat flux for January and July is shown in Fig. 5. The maps represent a smoothed composite of results by Budyko (1963) for land, Rusin (1964), Dalrymple et al. (1966) and Fletcher (1969) for the snow and ice-covered regions of the Antarctic and Privett (1960), Zillman (1972b, 1972c) plus other sources for the oceans (Zillman, 1972a).

The vertical apportionment of the sensible heat flux within the boundary layer is difficult to specify so a very simple model based on physical plausibility arguments was adopted (Zillman, 1972a). In areas where the sensible heat flux is upward, the vertical diabatic mass transport, $\rho J\dot{\theta}$, is assigned the value $[(H/20c_p) - 500 \times 10^{-6}]$ kg m^{-2} s^{-1} on $\bar{\theta}_a + 2.5$, $[(H/10c_p) + 500 \times 10^{-6}]$ kg m^{-2} s^{-1} on $\bar{\theta}_a - 2.5$, $(H/20c_p)$ kg m^{-2} s^{-1} on $\theta_a - 7.5$ and 0 on the other isentropes. In areas where the sensible heat flux is downward, the vertical mass transport is assigned the value $[(H/10c_p) - 500 \times 10^{-6}]$ kg m^{-2} s^{-1} on $\bar{\theta}_a + 2.5$, $(H/20c_p)$ kg m^{-2} s^{-1} on $\bar{\theta}_a + 7.5$, $[(H/20c_p) + 500 \times 10^{-6}]$ kg m^{-2} s^{-1} on $\bar{\theta}_a - 2.5$ and 0 on the other isentropes. In the

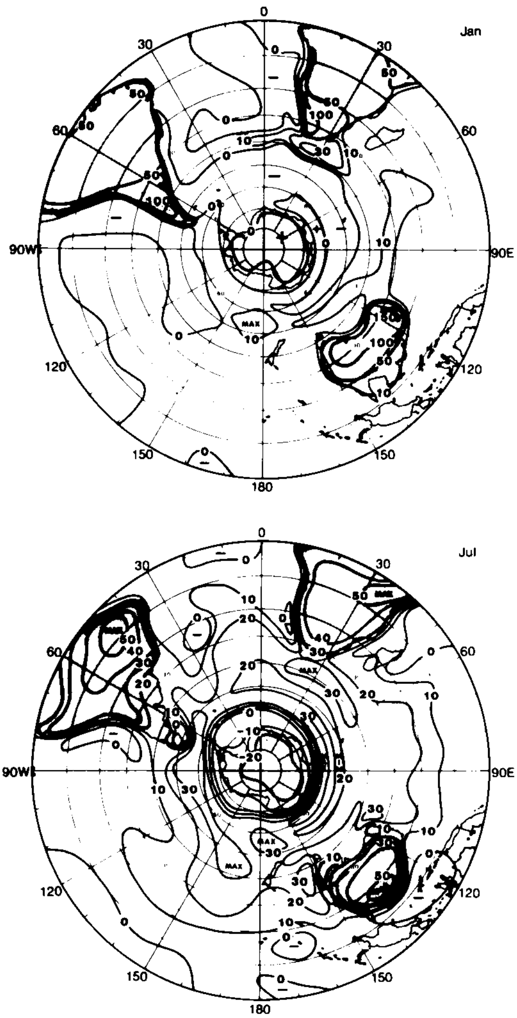

Fig. 5. Sensible heat flux to the atmosphere from the earth's surface in January (top) and July (bottom) in units of W m^{-2}.

special case when the net sensible heat flux is zero, the vertical diabatic mass flux is assigned the value -500×10^{-6} kg m^{-2} s^{-1} on the isentrope $\bar{\theta}_a + 2.5$ and $[+500 \times 10^{-6}]$ kg m^{-2} s^{-1} on $\bar{\theta}_a - 2.5$. Its magnitude decreases linearly (with θ) to zero on $\bar{\theta}_a + 7.5$ and $\bar{\theta}_a - 7.5$ and is zero on all other isentropes.

The somewhat arbitrary selection of numerical values for the heating on $\theta < \bar{\theta}_a$ and cooling on $\theta > \bar{\theta}_a$ for zero time-averaged heat flux was motivated by typical magnitudes of the positive and negative sensible heat fluxes in a region where this condition is prevalent, e.g., the Southern Ocean in summer (Zillman, 1972c). Quite obviously, this scheme represents a drastic oversimplification especially for the land areas. The approach is only tolerable within the context of the present study because for the physically plausible range of possibilities the assumed pattern of heating and cooling in the planetary boundary layer makes only a relatively minor contribution to the inferred three-dimensional mass circulation patterns.

3.5. *Adjustment for steady state*

In the steady-state condition, the hemispheric area-integrated vertical mass transport must vanish on isentropes which intersect the earth's surface and, for others, must equal the total rate of mass inflow from the Northern Hemisphere below the isentrope concerned. Since the components of the vertical mass transport were assembled independently of this constraint, an adjustment is necessary to derive model forcing fields consistent with the assumed steady condition. In the adjustment, the relative variation of the modeled diabatic heating with latitude along individual isentropes is preserved. The procedure consists of evaluating

$$\overline{[\rho J_\theta \dot{\theta}]}_{\mathrm{Adj}} = \overline{[\rho J_\theta]}[\bar{\dot{\theta}}] - \overline{[\rho J_\theta]} \left\{ \frac{\int_{-\pi/2}^{0} \overline{[\rho J_\theta]}[\bar{\dot{\theta}}] \cos\phi \, \mathrm{d}\phi - \dfrac{X}{2\pi a^2}}{\int_{-\pi/2}^{0} \overline{[\rho J_\theta]} \cos\phi \, \mathrm{d}\phi} \right\} \qquad (11)$$

where the square brackets indicate zonal averages and X is equal to the total rate of mass inflow from the Northern Hemisphere below the particular isentrope. Estimates of X at the equatorward boundary were derived from the mean poloidal mass circulation stream function computations of Oort and Rasmusson (1971) by direct mapping from isobaric coordinates. The approximately barotropic character of the inner tropics suggests that only slight differences between the mean poloidal mass circulations in the two coordinate systems will exist at the equator.

Cross sections of the adjusted estimates of the vertical mass transport are shown in Fig. 6. The

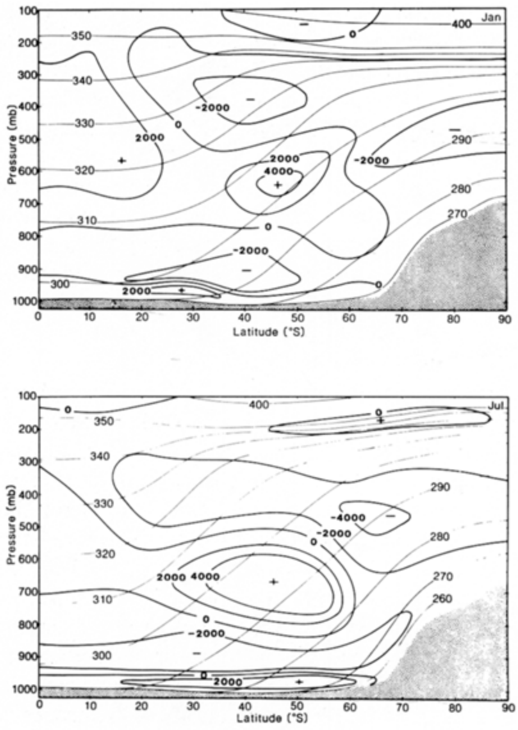

Fig. 6. Estimates for January (top) and July (bottom) of the zonally-averaged vertical mass transport after adjustment to satisfy the condition of steady-state mass distribution. The units are 10^{-6} kg m^{-2} s^{-1}.

areal distributions of the forcing function for the 280, 310 and 330 K isentropic surfaces are shown in Fig. 7. The adjustment determined from (11) was assigned solely to the radiative component and assumed longitudinally invariant. Although the adjustment process produced significant changes in magnitude, the broad features of the unadjusted fields were preserved. There is, of course, little reason to believe that individual point estimates from Fig. 6 are any nearer to the true values of the vertical mass transport than the preliminary estimates but the results of the adjustment process do constitute an internally consistent pattern that provides a suitable basis for determining the steady-state mass circulation.

4. Horizontal mass transport

Fig. 8 shows the distribution of the mass transport potential χ on the 280, 310 and 330 K isentropic surfaces for January (summer) and July (winter). These were obtained by solution of (4) using the forcing function fields given in Fig. 7.

The patterns of the mass transport potential χ determine the distribution of the irrotational (thermally-forced) component of the time-averaged horizontal mass transport

$$\overline{\rho J_\theta \mathbf{U}_\chi} = \nabla_\theta \bar{\chi}. \tag{12}$$

Its zonal and meridional components, respectively, are

$$\overline{\rho J_\theta u_\chi} = \frac{1}{a \cos \phi} \frac{\partial \bar{\chi}}{\partial \lambda_\theta} \tag{13}$$

$$\overline{\rho J_\theta v_\chi} = \frac{1}{a} \frac{\partial \bar{\chi}}{\partial \phi_\theta}. \tag{14}$$

The broad features of the thermally-forced horizontal mass transport are evident in Fig. 8. The mean pressure on these isentropic surfaces depicted may be inferred from Fig. 1. Note, however, that the quantities from which the mass transport potential is derived represent averages through a 10 K deep layer centered on the nominal isentrope. Thus, for example, mass transport is indicated "on" the 280 K surface in regions where this surface remains perpetually underground but where the 285 K surface does not.

4.1. *Summer distributions*

The meridional component of the horizontal mass transport tends to dominate on the three isentropic surfaces shown, as well as on most of the intermediate surfaces not shown. Nevertheless some quite marked zonal asymmetries exist particularly in association with the summer latent heat release maxima over southern Africa and South America and the band of heavy rainfall lying southeastward from Papua-New Guinea. Note the region of pronounced horizontal mass convergence in the lower troposphere (310 K surface) centered near 10° S, 170° E and the upper tropospheric (330 K surface) outflow centered further to the southeast. Note also the center of low-level inflow on the 280 K surface just west of the southern tip of South America and the region of outflow on the 310 K surface above. This toroidal circulation cell is associated with the center of high precipitation in this region. Centers of low-level inflow and high-level outflow are also

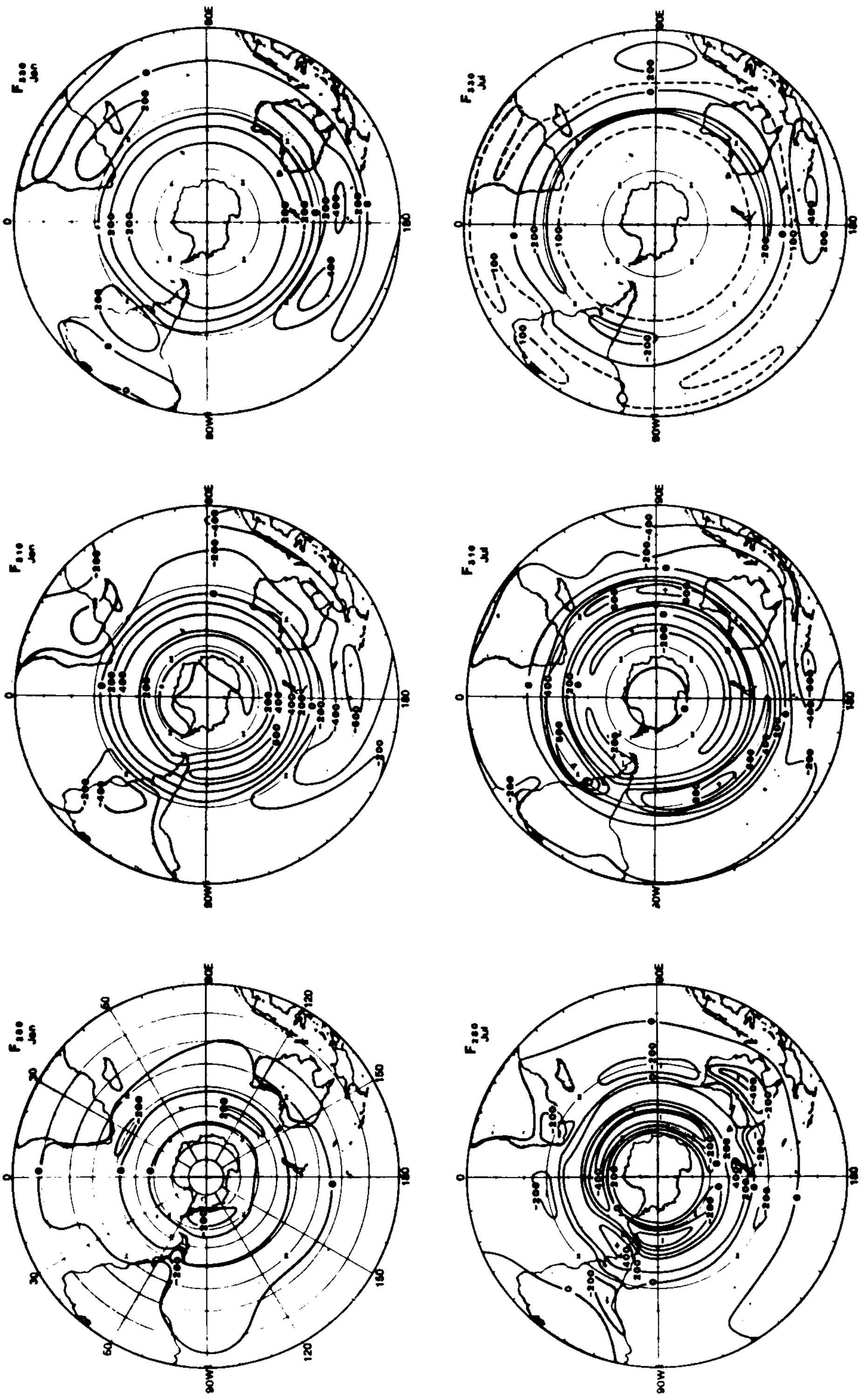

Fig. 7. The forcing function for January (top) and July (bottom) for the 280 K (left), 310 K (center), and 330 K (right) isentropic surfaces. The units are 10^{-6} kg m^{-2} K^{-1} s^{-1}.

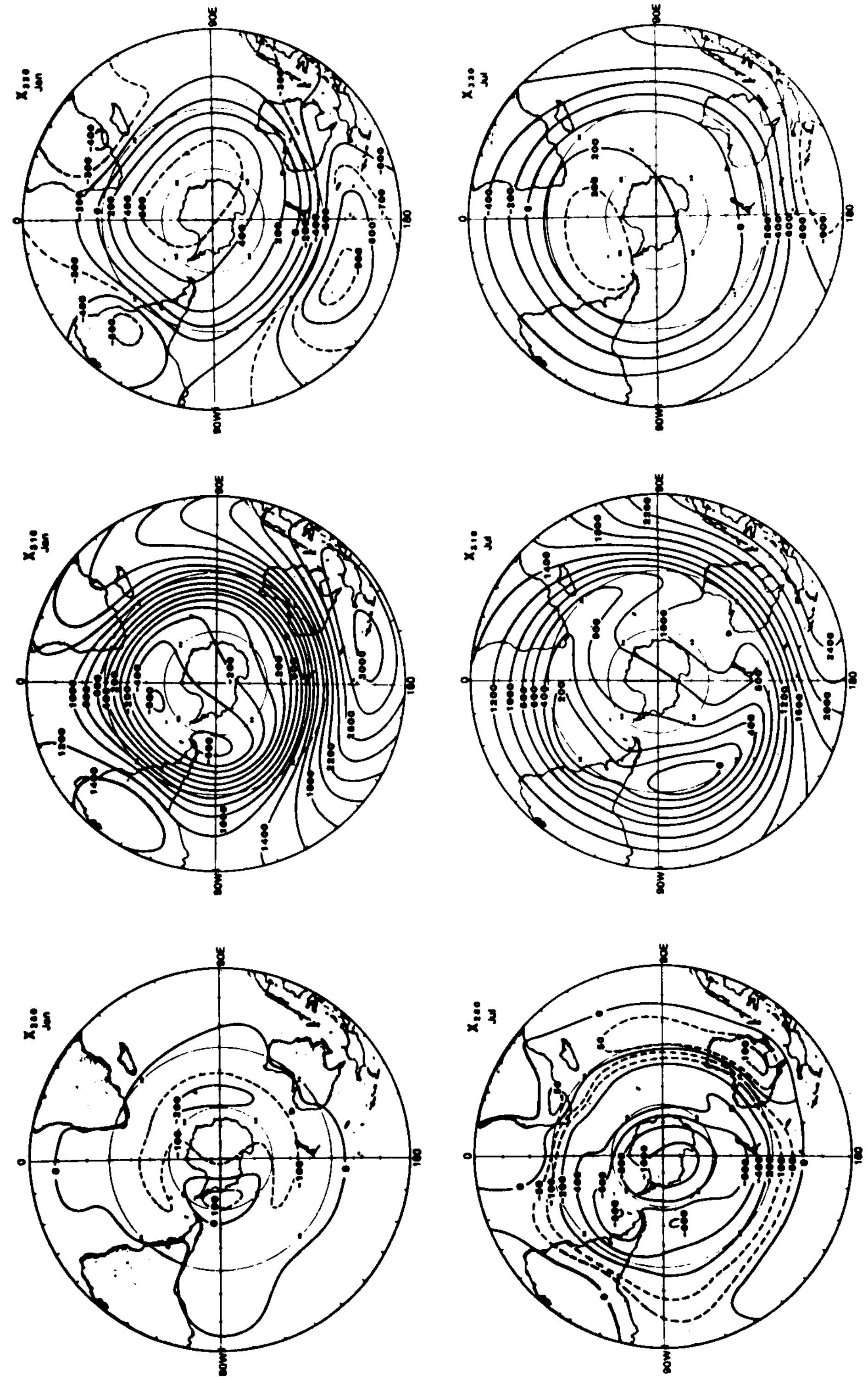

Fig. 8. The mass transport potential for January (top) and July (bottom) for the 280 K (left), 310 K (center), and 330 K (right) isentropic surfaces. The units are 10^6 kg k^{-1} s^{-1}.

evident over tropical South America. In general, the summer monsoonal circulations appear much less well developed in the Southern Hemisphere than was found in the studies for the Northern Hemisphere (Otto-Bliesner and Johnson, 1982) and for the global circulation (Johnson and Townsend, 1981).

4.2. *Winter distributions*

The changes in the patterns of horizontal mass transport from summer to winter appear mainly as minor shifts and changes of intensity of the main centers of inflow and outflow. For the most part these are not as dramatic as the corresponding summer to winter changes found for the Northern Hemisphere (Otto-Bliesner and Johnson, 1982).

The large-scale circulation cell over the Amazon basin in January is not evident in the July pattern and the centers of low-level inflow and high-level outflow in the tropical western Pacific are displaced well to the northwest of their summer positions. This seasonal displacement of the ascending branch of the Asiatic monsoon over the tropical western Pacific and southeast Asia is in agreement with Johnson and Townsend's (1981) results computed from FGGE data. The strong meridional and to some extent zonal gradient between southeast Asia and regions over Antarctica and the southeastern Pacific is indicative of the relatively intense isentropic mass circulation that links the Asiatic summer monsoon circulation with the Southern Hemisphere. On the 310 K isentropic surface, the irrotational component of the mass transport is from the Southern Hemisphere towards Southeast Asia while on the 330 K isentropic surface, the mass transport is directed from Southeast Asia towards the polar latitudes of the Southern Hemisphere. The influence of the strong net radiation cooling over the Antarctic ice cap and the sensible heating of cold air by the relatively warm circumpolar ocean is evident from the mass transport potential pattern on the 280 K surface.

5. East–west mass circulations

As far back as the 1920's Sir Gilbert Walker had drawn attention to the world-wide fluctuation of opposed pressure anomalies between the Eastern and Western Hemispheres (Walker, 1923; Walker and Bliss, 1932). However, Troup (1965) was the first to associate this 'Southern Oscillation,' so called because of its dominance in the Southern Hemisphere, with fluctuations in the strength of a solenoidally driven east–west mass circulation between the warmer Eastern and cooler Western Hemispheres. Bjerknes (1969, 1972) further developed the concept of a thermally driven east–west Walker circulation embedded within the tropical Hadley circulation; its main cell consisting of a region of ascent in the western Pacific linked by lower easterlies and upper westerlies to a region of descent off the west coast of South America. In a series of papers, Krishnamurti (1971a, b) and his coworkers (1973) identified some of the detailed structure of the tropical east–west circulations from actual wind data while Webster (1973) and Murakami (1974) examined their relation to prescribed patterns of thermal forcing using a two-layer linear and nine-layer linear model, respectively.

Within the constraints imposed by the truncation of the present model at 25° N, the solution for the divergent horizontal mass transport may be expected to provide a direct representation of the tropical Walker circulation and also to indicate the nature of its extension into higher latitudes of the Southern Hemisphere. Although the meridional components of flow dominate the mass transport patterns of Fig. 8, significant large-scale east–west circulations are also apparent and clearly associated with the zonal asymmetry of the adopted diabatic heating fields.

The three-dimensional structure of the east–west circulations is shown more explicitly in Fig. 9 which gives the spatial distribution of the thermally-forced zonal mass transport on the 280, 310 and 330 K isentropic surfaces. Since maps are presented for only these three isentropic surfaces, features which are confined to the intermediate layers in both seasons or which shift to higher valued isentropic surfaces from July to January (e.g., the center of westward mass transport over the southern tip of South America on the 280 K isentropic surface in July) are not completely depicted by this form of presentation. Some additional detail of the structure is provided by examining cross sections. Fig. 10 presents zonal cross sections along the equator and 30° S. The computed zonal mass transports at ten-degree intervals of potential temperature were plotted at the zonal mean pressure of the isentropic surface indicated at the

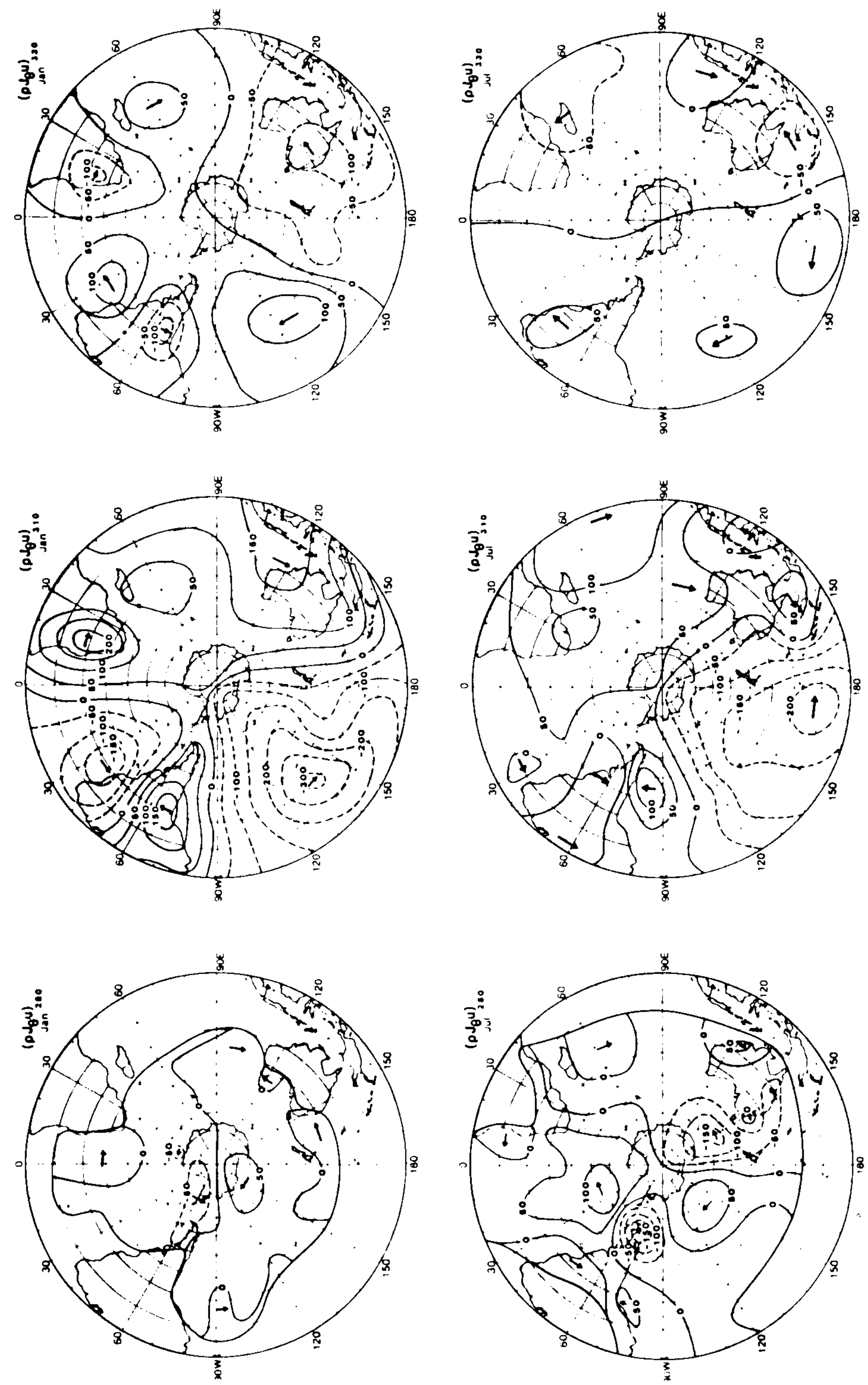

Fig. 9. The zonal component of the time-averaged irrotational horizontal mass transport for January (top) and July (bottom) for the 280 K (left), 310 K (center), and 330 K (right) isentropic surfaces. The units are kg m^{-1} K^{-1} s^{-1}.

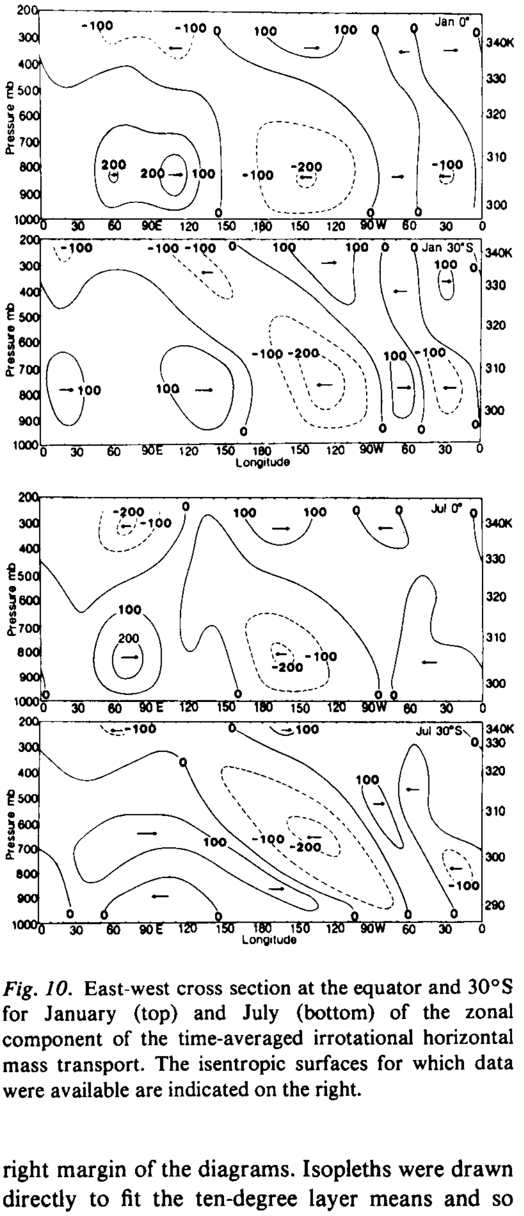

Fig. 10. East-west cross section at the equator and 30°S for January (top) and July (bottom) of the zonal component of the time-averaged irrotational horizontal mass transport. The isentropic surfaces for which data were available are indicated on the right.

right margin of the diagrams. Isopleths were drawn directly to fit the ten-degree layer means and so the patterns underestimate vertical gradients and extremes. Also, since the effect of terrain on the vertical distribution of latent heat release and stability was not taken into account when specifying the spatial distribution of the forcing function, the patterns are not realistic below or near elevated terrain (e.g., the South American Andes).

The equatorial cross sections of Fig. 10 capture the gross features of the Walker circulation as depicted by previous authors (e.g., Flohn, 1971; Krishnamurti et al., 1973; Newell et al., 1974) and are also, as should be expected, in broad agreement with the results of the counterpart study for the Northern Hemisphere (Otto-Bliesner and Johnson, 1982). Fig. 11 compares the thermally-forced mass-weighted mean zonal velocity on the 340 K surface at the equator (the highest evaluated in the present study, at approximately 300 mb) with the mean irrotational zonal velocity at 200 mb, for June, July and August 1967 computed from velocity potentials read at ten-degree intervals of longitude from the map of Krishnamurti (1971a). The patterns are quite similar in the Eastern Hemisphere but differ in the Western Hemisphere. Most conspicuously Krishnamurti's study suggests high-level easterlies over the eastern Pacific with subsidence in mid-ocean whereas in these results the upper westerlies over the Pacific extend almost to 90° W. The Pacific cell of low-level easterlies and upper westerlies in Figs. 9 and 10 is matched by an equally strong cell in the reverse sense over the tropical Indian Ocean. Weaker circulation cells are associated with the other zonal asymmetries in the precipitation patterns. The effect of the summer rainfall maxima over South America and southern Africa is evident, for example, in the January cross section for 30° S.

Outside the tropical belt the major east–west circulation cell in both seasons appears to consist of a poleward extension, eastward shift and longitudinal constriction of the low-level easterlies and overriding westerlies of the equatorial Pacific. The reverse cell over the equatorial Indian Ocean also shows a pronounced eastward shift at higher latitudes when mapped into isobaric coordinates. In

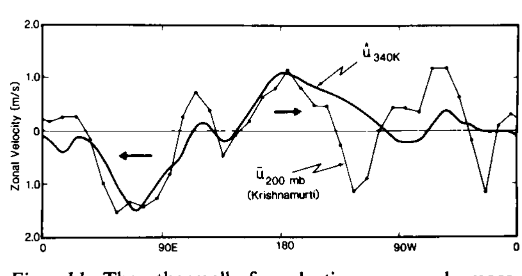

Fig. 11. The thermally-forced time-averaged mass-weighted zonal velocity $\hat{u}(=\overline{\rho J_\theta U}/\overline{\rho J_\theta})$ at the equator on the 340 K isentropic surface in July (solid curve) compared with the zonal component of the divergent velocity field on the 200 mb surface for June–July–August 1967 computed from Krishnamurti (1971b).

the cross section for 45° S (not shown) the two cells appear juxtaposed in the eastern Pacific in response to the strong latent heating maximum near 90° W.

6. Meridional mass circulations

The distribution of the mass transport potential in Fig. 8 and on various other isentropic surfaces not presented shows that, at most latitudes, the meridional component of the thermally-forced mass transport is dominant and that it varies considerably with longitude. The zonally-averaged meridional (poloidal) circulation and the variation with longitude of the time-averaged thermally forced meridional flow are now considered.

6.1. *The mean poloidal mass circulation*

A zonal average of the potential $\bar{\chi}$ or of the derived meridional component of the mass transport provides a description of the mean poloidal component of the mass circulation in isentropic coordinates. However, since the relaxation solution for χ is only an approximate procedure and the computed mass transports refer to averages through 10 K layers, it is more convenient to determine the mean meridional mass transport directly from the adjusted vertical mass transport by an application of the divergence theorem to the equation of continuity. With an integration of the zonally time-averaged distribution of heating over the polar cap, the meridional mass transport is

$$\overline{\rho J_\theta v} = -\frac{a}{\cos\phi}\int_{-\pi/2}^{\phi}\frac{\partial}{\partial\theta}\overline{\rho J_\theta\dot{\theta}}\cos\phi'\,\mathrm{d}\phi'. \tag{15}$$

A stream function (S) for the mean poloidal mass circulation defined by

$$2\pi a\cos\phi\,\overline{\rho J_\theta v} = -\frac{\partial S}{\partial\theta} \tag{16}$$

and

$$2\pi a^2\cos\phi\,\overline{\rho J_\theta\dot{\theta}} = \frac{\partial S}{\partial\phi} \tag{17}$$

is readily evaluated from the data of Fig. 6 by

$$S = 2\pi a^2\int_{-\pi/2}^{\phi}\overline{\rho J_\theta\dot{\theta}}\cos\phi'\,\mathrm{d}\phi'. \tag{18}$$

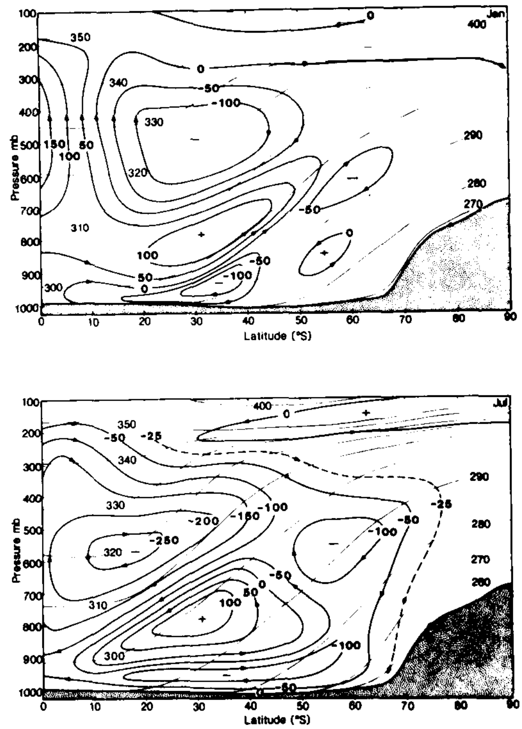

Fig. 12. The streamfunction for the mean poloidal mass circulation in isentropic coordinates for January (top) and July (bottom) implied by the modeled diabatic heating after adjustment for steady-state mass distribution. The units are 10^9 kg s^{-1}.

The numerical integration was performed for each 5 K isentrope from 250 K to 380 K using five-degree increments of latitude. The resulting streamlines mapped in isobaric coordinates for January and July are shown in Fig. 12. Note, however, that the stream function cannot be interpreted apart from the superposed isentropes. The mass flow in each streamline channel is 5×10^{10} kg s^{-1}.

The dominant features in both seasons are: a large Hadley cell centered near the 320 K isentrope that spans the low and middle latitudes; an embedded reverse cell centered at lower potential temperature and clearly coupled to the latent heating maximum over the Southern Ocean; and a shallow Hadley cell spanning the entire latitude belt in winter but restricted to low and middle latitudes in summer. The upper Hadley cell is located near 20° S in January and 30° S in July. Its strength doubles from summer to winter. The shallow circulation cells transecting the near surface isentropes appear in Fig. 12 as a combined result of the assignment of most of the boundary layer sensible heating to isentropes colder than the mean surface potential temperature and the influence of cooling by infrared emission and by the modeled downward sensible heat flux in layers immediately above.

It is difficult to say what level of confidence should be placed in any of the detailed cell structures of Fig. 12. The stream function isopleths are those required by the principle of mass conservation to accord with the modeled diabatic heating and vertical mass transport patterns. The assembly of the latter, however, involved several approximations and rather arbitrary selection from conflicting data and viewpoints. The strong counter-Hadley cells in the lower middle latitude troposphere and the shallow "direct" cells beneath them are the result of the large precipitation maximum over the Southern Ocean (moderately well documented), the assumption on the vertical apportionment of latent heat release (somewhat uncertain) and the model of sensible heating (an oversimplification). The existence of an isentropic layer subject to strong net cooling between the surface-heated isentropic surfaces and those on which the bulk of the latent heat release occurs (Fig. 6) is questionable. If, in fact, the longwave radiative cooling dominates the other two components on some such intermediate isentropic surface, the small-scale vertical eddy redistribution of enthalpy (Palmén, 1966) may well dominate the large-scale mass circulation in compensating the radiative cooling. In this circumstance the lower negative regions in Fig. 6 could conceivably disappear completely with the positive regions above simultaneously weakened.

An approximation to this condition and the basis for an indication of the uncertainty of the mean poloidal circulation of Fig. 12 is provided by the pole-to-pole cross sections of net diabatic heating for December to February and June to August given by Newell et al. (1969). Evaluation of the mean poloidal mass circulation was carried out as for Fig. 12 except that the sensible heating was mapped, along with the other components, directly from isobaric coordinates. As before, the vertical mass transports were adjusted to accord with the transequatorial mass flow given by Oort and Rasmusson (1971). The required adjustments to the preliminary estimates of diabatic mass flux were quite large, partly because, as noted by Newell et al. (1969), their heating cross sections imply net global cooling in both seasons. The derived mean poloidal mass circulation superposed on the isentropes mapped into isobaric coordinates is given in Fig. 13. The Hadley component of the circulation is quite prominent in both hemispheres and both seasons while the counter-Hadley cells of Fig. 12 are virtually absent. In this respect the mass circulations implied by Fig. 13 are in better agreement with the findings of Townsend and Johnson (1981) determined from an analysis of an NMC FGGE Level IIIa data set.

6.2. *Longitudinally varying meridional circulation*

The patterns of the mass transport potential in Fig. 8 suggest that the longitudinally varying standing eddy component of the time-averaged meridional circulation is not small. This is confirmed by Fig. 14 which shows the longitudinal variation of the mass-weighted time-averaged meridional velocity. At the equator in July the meridional circulation is even reversed over a thirty-degree longitude sector where the precipitation maximum lies southeast from Papua-New Guinea. At higher latitudes also, significant longitudinal variation is apparent. This is illustrated for 30° S in Fig. 14 for both January and July. For July, the 300 and 330 K isentropic surfaces replace the 310 and 340 K surfaces used at the equator.

The main features of Fig. 14 can be recognized also in the results of the Northern Hemisphere study (Otto-Bliesner and Johnson, 1982) but, in general, the degree of quantitative agreement at the equator is disappointing and underscores the advantage of a single pole-to-pole evaluation to define more precisely the thermally-forced circulation in the equatorial belt.

7. Energy transport by the mean mass circulation

One of the most important atmospheric responses due to the physical forcing by differential heating is the transport of energy between planetary-scale heat sources and sinks. It is particularly important in the determination of climate, since the energy transport maintains quasi-

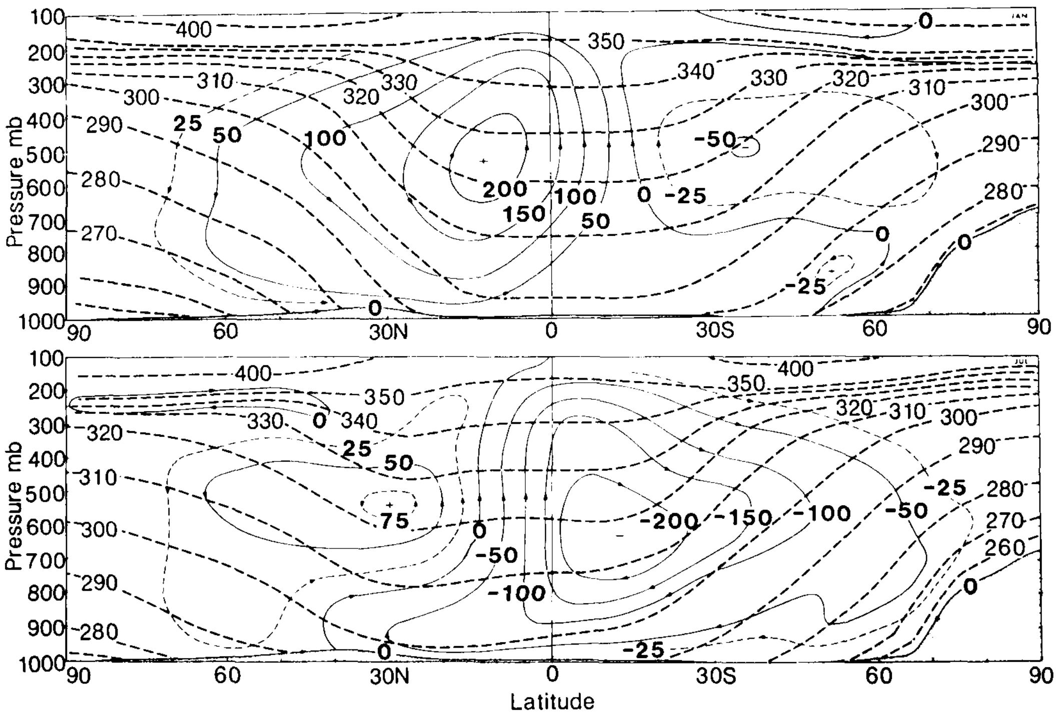

Fig. 13. The streamfunction for the mean poloidal mass circulation in isentropic coordinates for January (top) and July (bottom) based on the total diabatic heating cross sections of Newell et al. (1969) and the transequatorial flow estimates of Oort and Rasmusson (1971). The units are 10^9 kg s^{-1}.

steady state temperature distributions which are more moderate than would be attained if the atmosphere were to achieve local radiative equilibrium in the absence of transport. Current theory based on isobaric analysis strongly implies that eddy scales provide for, and in turn force, the energy transport. An analysis by Johnson and Townsend (1981) strongly suggests that a thermally-forced mean mode of energy transport exists in concert with the thermally-forced mass transport. The results for the mass circulation presented in the previous sections establish that both Hadley and Walker type circulations are actual components of the three-dimensional planetary-scale response to global differential heating. The aim of the following analysis of the isentropic transport equation is to demonstrate the important role of thermally-forced mass circulations in energy transport at the planetary scale.

The role of the meridional components of the circulation in effecting a net poleward energy transfer can readily be inferred from the patterns of the mass transport potential in Fig. 8 and can be evaluated quantitatively from Fig. 12. The total poleward energy transfer across a latitude wall is, to a close approximation,

$$B_\phi(e) = 2\pi a \cos\phi \int_0^\infty \overline{\rho J_\theta v \psi}\, \mathrm{d}\theta. \tag{19}$$

Because of the choice of 1000 mb as the reference pressure for the definition of potential temperature and in consequence of the approximate geostrophic and hydrostatic balance of the atmosphere, ψ may be replaced by $c_p\theta$ in (19) with negligible additional error for the present purpose. The poleward energy transfer then takes the form

$$B_\phi(e) = 2\pi a \cos\phi\, c_p \int_0^\infty \overline{\rho J_\theta v \theta}\, \mathrm{d}\theta \tag{20}$$

$$= c_p \int_0^\infty S\, \mathrm{d}\theta \tag{21}$$

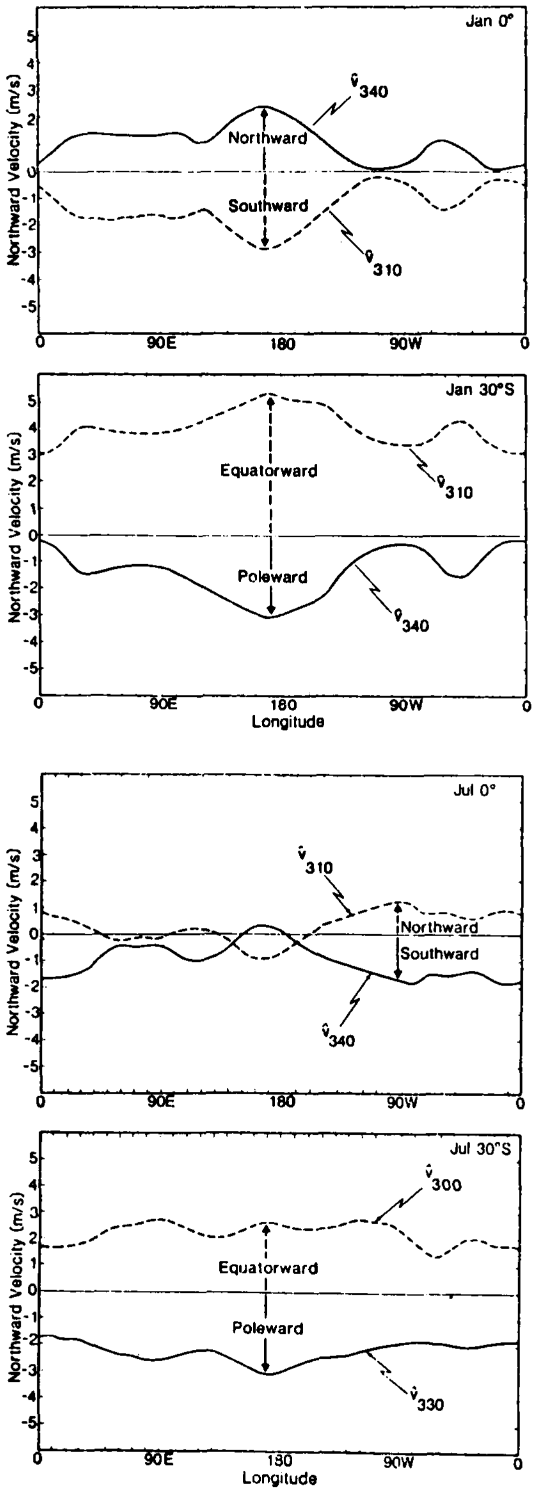

where S is the stream function of the mean poloidal mass circulation defined by (16) and (17).

Fig. 15 shows the meridional energy transport by the mean poloidal circulation of Fig. 12 computed according to (21) for each five degrees of latitude. This may be compared with the balance requirement (broken lines) based on the initially specified latitudinal distribution of energy sources and sinks (Fig. 16). The discrepancy is due mainly to two factors. Firstly, the storage term of the energy balance has been disregarded for January and July and this is only approximately valid. Secondly, the mass circulations of Fig. 12 are based on diabatic heating fields (specifically the radiation term) that were adjusted from the values given in Fig. 16 in accord with the steady-state mass assumption (eq. (2)). A complete solution for the poleward energy transfer would include the contribution by transient eddy fluxes. However, a preliminary assessment of isentropic eddy transfer of energy from rawinsonde data in the Australian sector (Zillman, 1972a) confirms that it is an order of magnitude less than the mean mass circulation contribution and may be expected to be unimportant for the planetary scale.

In addition to the meridional energy transfer, it is evident, from the pattern of the mass transport potential (Fig. 8), that the thermally-forced mass circulation also effects significant transfer of energy in the east–west direction between the major zonally distributed heat sources and sinks. For example the Pacific cell of the tropical Walker circulation transfers large amounts of energy from a strong source region northeast of Australia to the energy sink off the coast of Peru.

While the conclusions on energy transport are only qualitative and tentative, the results are consistent with current understanding of energy balance mechanisms. Additional studies are needed to firmly establish the combined role of thermally forced mass and energy transport at the planetary scale and even more importantly provide insight into their fundamental roles in the determination of the planetary scale of climate.

Fig. 14. The variation with longitude of the mass-weighted mean northward velocity $\hat{v}(=\overline{\rho J_\theta v}/\overline{\rho J_\theta})$ on the 310 K and 340 K isentropic surfaces at the equator and 30° S for January (top); and on the 310 K and 330 K isentropic surfaces in July (bottom). The velocities are in m s^{-1}.

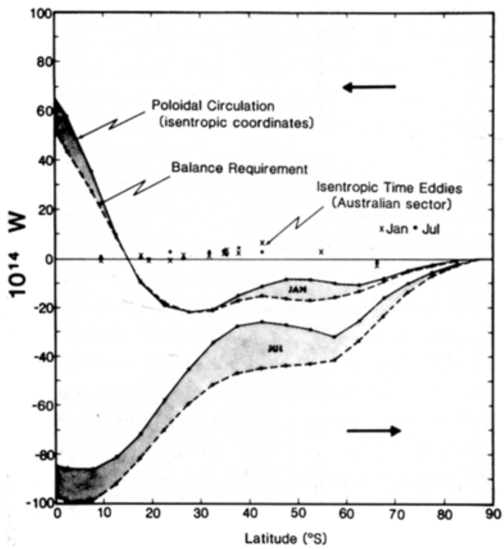

Fig. 15. Poleward energy transfer by the poloidal mass circulation shown in Fig. 12 for January and July (broken lines) compared with that required to balance the initially assumed meridional distribution of energy sources and sinks shown in Fig. 16 with energy storage rate assumed equal to zero (solid lines).

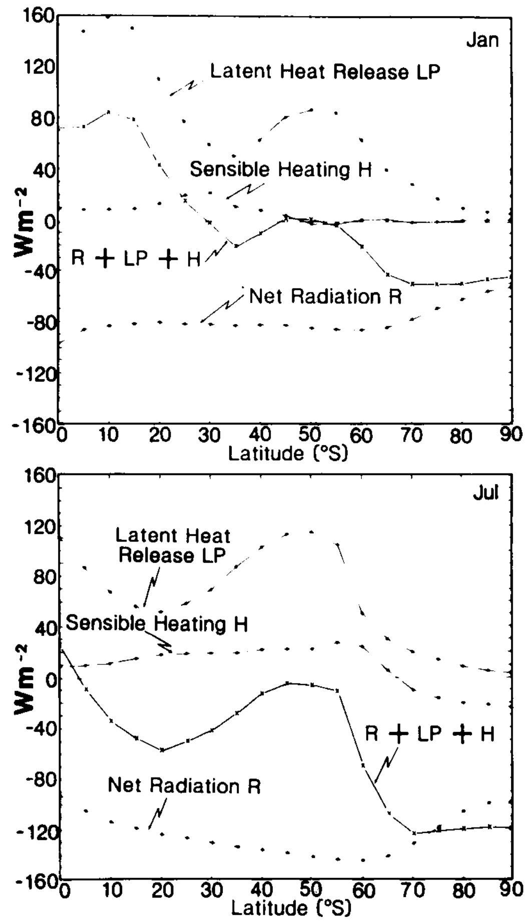

Fig. 16. Energy balance of the southern hemisphere in January (top) and July (bottom). The columnar radiant, latent and sensible heating components are compatible with the data of Figs. 2–5.

8. Conclusion

The main objective of this study was to develop a framework for isolating the three-dimensional structure of quasi-steady thermally-forced mass circulations in isentropic coordinates from climatological information and to use the approach to gain insight into the thermodynamics of the large-scale circulation features of the Southern Hemisphere.

Within the broad framework of the evolving theory of the general circulation in isentropic coordinates, several interesting results have emerged. It is clear that, in isentropic coordinates, three-dimensional time-averaged mass circulations link the large-scale zonally and latitudinally distributed heat sources and sinks and effect the greater part of the energy transfer needed to offset local heating and cooling. Thus, these circulations play a fundamental role in the determination of climate. The time and zonally-averaged meridional circulations in isentropic coordinates are found to be fundamentally different from the well documented three cell structure of isobaric coordinates. In isentropic coordinates a Hadley circulation spans the middle and high latitudes in summer and the complete hemisphere in winter. The time-averaged east–west circulations, although weaker than those in meridional planes, effect significant energy transfer between the zonally-aligned heat sources (principally the major rainbelts, to a lesser extent the solar heated continents) and heat sinks (predominant longwave radiative cooling over the ocean and deserts). The largest influence is exerted by the band of heavy precipitation extending from Indonesia into the western Pacific. It induces (or is induced by—direct cause and effect relationships are not isolated) two strong zonal circulation cells which extend across the entire latitude band and which appear in equatorial latitudes as the Walker circulation of isobaric coordinates. It appears that shifts and fluctuations of these circulation cells are intimately associated with the behavior of the Southern Oscillation, the development of the El Niño phenomenon and other features of the large-scale variability of climate.

While the key findings of this study are believed to be valid, limited confidence should be placed in the detail of the derived circulation patterns. At the outset of the original study (Zillman, 1972a) it became clear that the absence of data directly suited to the subtleties of isentropic coordinates, the inadequate state of conventional Southern Hemisphere climatology and the sheer effort of assembling substitute information precluded a definitive treatment. The main limitations of the data source, the techniques and some suggestions for the design of a more definitive evaluation are summarized in Zillman (1972a). In view of the uncertainities of energy transport that are emerging from use of FGGE data (Kung and Tanaka, 1983), an attempt to conduct a more definitive evaluation that relates energy balance of the Southern Hemisphere to thermally forced isentropic mass transport should be considered, particularly as it relates to the phenomenon of El Niño.

9. Acknowledgments

We express our appreciation to Thomas Whittaker for his computer programming and data processing assistance, to Dawn Zillman and Robert Clement for preparation of figures, and to Nancy Malz and Gail Turluck for typing the manuscript. This research was supported by The National Science Foundation, Atmospheric Research Section Grant GA-30978X, and National Science Foundation and the National Oceanic and Atmospheric Administration under Grant Number ATM82-09757. The first author's opportunity for study at the University of Wisconsin was sponsored through an Australian Commonwealth Public Service Board Postgraduate Scholarship.

REFERENCES

Bjerknes, J. 1969. Atmospheric teleconnections from the equatorial Pacific. *Mon. Wea. Rev. 97*, 163–172.

Bjerknes, J. 1972. Large-scale atmospheric response to the 1964–65 Pacific equatorial warming. *J. Phys. Oceanogr. 2*, 212–217.

Bjerknes, V., Bjerknes, J., Solberg H. and Bergeron, T. 1933. *Physikalische Hydrodynamik*. Springer, Berlin, 797 pp.

Budyko, M. I. 1963. *Atlas of the heat balance of the Earth*. (In Russian.) Kartfabrika Gosgeoltehizdata, Leningrad, 69 pp.

Crutcher, H. L., Jenne, R. L., Taljaard, J. J. and van Loon, H. 1971. *Climate of the upper air, Southern Hemisphere: Vol. 4, selected meridional cross sections of temperature, dew point and height, cross sections at 30° intervals around hemisphere.* Environmental Data Service, National Climatic Center, Asheville, NC, 60 Figs.

Dalrymple, P., Lettau, H. and Wollaston, S. 1966. South Pole micrometerology program data analysis. *Studies in antarctic meteorology* (ed. M. J. Rubin). Antarctic Res. Ser., 9, AGU, Washington, 13–58.

Dopplick, T. G. 1970. Global radiative heating of the earth's atmosphere. Planetary Circulations Project Report, No. 24, Contract AT(30-1)2241, [NTIS.MIT-2241-58], 36 pp.

Dutton, J. A. and Johnson, D. R. 1967. The theory of available potential energy and a variational approach to the atmospheric energetics. *Advances in geophysics*, Vol. 12. Academic Press, 333–346.

Eckart, C. 1960. *Hydrodynamics of oceans and atmospheres*. Pergamon Press, New York, 290 pp.

Fletcher, J. O. 1969. Ice extent on the Southern Ocean and its relation to world climate. RM-5793-NSF, Rand Corporation, Santa Monica, CA, 108 pp.

Flohn, H. 1971. Tropical circulation pattern. *Bonner Meteorol. Abh. 15*, 55 pp.

Jeffreys, 1933. The function of cyclones in the general circulation. *Proces—Verbaux de l'Association de Meteorologie, UGGI (Lisbon), Part II (Memoires)*, 219–230.

Johnson, D. R. and Townsend, R. D. 1981. Diagnostics of the heat sources and sinks of the Asiatic monsoon and the thermally-forced planetary scale. *ICSU/WMO GARP Conf. Proc. of Int. Conf. on Preliminary FGGE Data Analysis and Results*, 23–27 June 1980, Bergen, Norway, Geneva, 1981, 523–533.

Katayama, 1967. On the radiation budget of the troposphere over the Northern Hemisphere, II. *J. Meteorol. Soc. Japan 45*, 1–25.

Krishnamurti, T. N. 1971a. Observational study of the tropical upper tropospheric motion field during the

Northern Hemisphere summer. *J. Appl. Meteorol. 10*, 1066–1095.

Krishnamurti, T. N. 1971b. Tropical east–west circulations during the northern summer. *J. Atmos. Sci. 28*, 1342–1347.

Krishnamurti, T. N., Kanamitsu, M., Koss, W. J. and Lee, J. D. 1973. Tropical east–west circulations during the northern winter. *J. Atmos. Sci. 30*, 780–787.

Kuhn, P. M., Stearns, L. P. and Stremikis, J. R. 1967. Atmospheric infrared radiation over the Antarctic. ESSA Tech. Rept., IER 55-AIS 2, 75 pp.

Kung, E. C. and Tanaka, H. 1983. Energetic Analysis of the Global Circulation during the Special Observation Periods of FGGE. *J. Atmos. Sci. 40*, 2575–2592.

Lorenz, E. N. 1967. *The nature and theory of the general circulation of the atmosphere.* World Meteorological Organization, Geneva, No. 218, TP115, 161 pp.

Möller, F. 1951. Vierteljahrskarten des Niederschlags für die Ganze Erde. *Petermanns Geogr. Mitt. 95*, 1–7.

Murakami, T. 1974. Atmospheric response to heat sources during July. UHMET 74-04. Department of Meteorology, University of Hawaii, Honolulu. 56 pp.

Newell, R. E., Kidson, J. W., Vincent, D. G. and Boer, G. J. 1974. *The general circulation of the tropical atmosphere and interactions with extratropical latitudes,* Vol. 2. MIT Press, Cambridge, MA, 371 pp.

Newell, R. E., Vincent, D. G., Dopplick, T. G., Feruzza, D. and Kidson, J. W. 1969. The energy balance of the global atmosphere. *The global circulation of the atmosphere* (ed. G. A. Corby). Roy. Meteor. Soc. London, 42–90.

Newton, C. W. 1972. Southern hemisphere general circulation in relation to global energy and momentum balance requirements. *Meteorology of the Southern Hemisphere, Meteorol. Monogr. 13*, 350 pp.

Oort, A. H. and Rasmusson, E. M. 1971. Atmospheric circulation statistics. Environmental Research Labs, Princeton, NJ, Geophysical Fluid Dynamics Lab. NOAA Professional Paper, 5, NOAA-72032903, [NTIS.COM-72-50295], 335 pp.

Otto-Bliesner, B. L. and Johnson, D. R. 1982. Thermally-forced mean mass circulation in the Northern Hemisphere. *Mon. Wea. Rev. 110*, 916–932.

Palmén, E. 1949. Meridional circulations and the transfer of angular momentum in the atmosphere. *J. Meteorol. 6*, 429–430.

Palmén, E. 1966. On the mechanism of the vertical heat flux and generation of kinetic energy in the atmosphere. *Tellus 18*, 838–845.

Priestley, C. H. B. 1949. Heat transport and zonal stress between latitudes. *Q. J. R. Meteorol. Soc. 75*, 28–40.

Privett, D. W. 1960. The exchange of energy between the atmosphere and the oceans of the southern hemisphere. *Geophys. Mem.*, London, *13*, 61 pp.

Riehl, H. 1969. Mechanisms of the general circulation of the troposphere. *World survey of climatology*, 2 (ed. D. F. Rex). Elsevier, Amsterdam, 1–37.

Riehl, H. and Yeh, T. C. 1950. The intensity of the net meridional circulation. *Q. J. R. Meteorol. Soc. 76*, 182–188.

Rossby, C. G. and Starr, V. P. 1949. Interpretations of the angular-momentum principle as applied to the general circulation of the atmosphere. *J. Meteorol. 6*, 288.

Rusin, N. P. 1964. Meteorological and radiational regime of Antarctica. Israel Program for Scientific Translations, Jerusalem, 355 pp. (original Russian text, 1961, Leningrad).

Sasamori, T., London, J. and Hoyt, D. V. 1971. Radiation budget of the southern hemisphere. *Meteorology of the Southern Hemisphere, Meteorol. Monogr. 13.*

Schwerdtfeger, W. 1969. The climate of the antarctic. *World survey of climatology*, 14 (ed. S. Orvig). Elsevier, Amsterdam, 153–355.

Sellers, W. D. 1965. *Physical climatology.* University of Chicago Press, Chicago, 272 pp.

Smagorinsky, J. 1953. The dynamical influence of large-scale heat sources and sinks on the quasi-stationary mean motions of the atmosphere. *Q. J. R. Meteorol. Soc. 79*, 342–366.

Starr, V. P. 1951. A note on the eddy transport of angular momentum. *Q. J. R. Meteorol. Soc. 77*, 44–50.

Taljaard, J. J., van Loon, H., Crutcher, H. L. and Jenne, R. L. 1969. Temperatures, dew points and heights at selected pressure levels. *Climate of the upper air: Southern Hemisphere*, Vol. I, NAVAIR 50-1C-55, Chief of Naval Operations, Washington, DC, 135 pp. [Commander, Naval Weather Services Command, Washington Navy Yard, Bldg. 200, Washington, DC, 20390.]

Townsend, R. D. 1980. A diagnostic study of the zonally-averaged global circulation in isentropic coordinates. Ph.D. thesis, Department of Meteorology, University of Wisconsin-Madison, 221 pp.

Townsend, R. D. and Johnson, D. R. 1981. The mass and angular momentum balance of the zonally-averaged global circulation. *ICSU/WMO GARP Conf. Proc. of Int. Conf. on Preliminary FGGE Data Analysis and Results* (Bergen, Norway), WMO, Geneva, 542–552.

Troup, A. J. 1965. The "Southern Oscillation." *Q. J. R. Meteorol. Soc. 91*, 490–506.

Vincent, D. G. 1969. Seasonal changes in the global atmospheric energy balance and results for restricted regions. Ph.D. thesis, Department of Meteorology, Massachusetts Institute of Technology, 174 pp.

Walker, G. T. 1923. A preliminary study of world weather-correlation in seasonal variations of weather, VIII. *Mem. India Meteorol. Dept. 24*, 75–131.

Walker, G. T. and Bliss, E. W. 1932. World Weather V. *Mem. R. Meteorol. Soc. 4*, 53–84.

Webster, P. J. 1973. Temporal variation of low-latitude zonal circulations. *Mon. Wea. Rev. 101*, 803–816.

White, F. D. and Bryson, R. A. 1967. The radiative factor in the mean meridional circulation of the

Antarctic atmosphere during the polar night. *Proc. of the Symp. on Polar Meteor.*, Geneva, 1966, World Meteorological Organization, Tech. Note, 87, 199–224.

Zillman, J. W. 1972a. Isentropically time-averaged mass circulations in the Southern Hemisphere. Ph.D. thesis, University of Wisconsin-Madison, 205 pp.

Zillman, J. W. 1972b. A study of some aspects of the radiation and heat budgets of the Southern Hemisphere oceans. Meteor. Study No. 20, Bureau of Meteor., Australian Government Printing Service, Canberra, 502 pp.

Zillman, J. W., 1972c. Solar radiation and sea–air interaction south of Australia. American Geophysical Union, Antarctic Research Series, 19, 11–40.